THE JOURNAL OF BIOLOGICAL CHEMISTRY VOL. 284, NO. 2, pp. 1018–1030, January 9, 2009

Cadherin Switching and Activation of β-Catenin Signaling Underlie Proinvasive Actions of Calcitonin-Calcitonin Receptor Axis in Prostate Cancer*[S]

Received for publication, October 10, 2008, and in revised form, November 3, 2008 Published, JBC Papers in Press, November 9, 2008, DOI 10.1074/jbc.M807823200

Girish V. Shah[1], **Anbalagan Muralidharan, Mitan Gokulgandhi, Kamal Soan, and Shibu Thomas**

From the Department of Pharmacology, University of Louisiana College of Pharmacy, Monroe, Louisiana 71209

Calcitonin, a neuroendocrine peptide, and its receptor are localized in the basal epithelium of benign prostate but in the secretory epithelium of malignant prostates. The abundance of calcitonin and calcitonin receptor mRNA displays positive correlation with the Gleason grade of primary prostate cancers. Moreover, calcitonin increases tumorigenicity and invasiveness of multiple prostate cancer cell lines by cyclic AMP-dependent protein kinase-mediated actions. These actions include increased secretion of matrix metalloproteinases and urokinase-type plasminogen activator and an increase in prostate cancer cell invasion. Activation of calcitonin-calcitonin receptor autocrine loop in prostate cancer cell lines led to the loss of cell-cell adhesion, destabilization of tight and adherens junctions, and internalization of key integral membrane proteins. In addition, the activation of calcitonin-calcitonin receptor axis induced epithelial-mesenchymal transition of prostate cancer cells as characterized by cadherin switch and the expression of the mesenchymal marker, vimentin. The activated calcitonin receptor phosphorylated glycogen synthase kinase-3, a key regulator of cytosolic β-catenin degradation within the WNT signaling pathway. This resulted in the accumulation of intracellular β-catenin, its translocation in the nucleus, and transactivation of β-catenin-responsive genes. These results for the first time identify actions of calcitonin-calcitonin receptor axis on prostate cancer cells that lead to the destabilization of cell-cell junctions, epithelial-to-mesenchymal transition, and activation of WNT/β-catenin signaling.The results also suggest that cyclic AMP-dependent protein kinase plays a key role in calcitonin receptor-induced destabilization of cell-cell junctions and activation of WNT-β-catenin signaling.

Prostate cancer (PC)[2] is the most commonly diagnosed cancer and the second leading cause of cancer deaths in men in the United States (1, 2). Although androgen ablation therapy is effective in men with advanced disease for some time, the disease subsequently progresses to the androgen-independent stage. The population of prostate cells expressing neuroendocrine factors such as calcitonin (CT) also increases during this progression (3–5). At this stage, the disease is metastatic and chemoresistant. Present evidence suggests that cancer metastasis is usually preceded by the disruption of normal cell-cell adhesion and the loss of integrity of the primary tumor site (6, 7). This process may include several genetic, molecular, and morphological changes characterized by epithelial-to-mesenchymal transition (EMT) (8–10). The EMT is characterized by the loss of cell polarity, altered cell-cell and cell-matrix adhesion, and acquisition of migratory, mesenchymal phenotype. Other reported changes include down-regulation of E-cadherin, induction of N-cadherin, release of β-catenin from junctional complexes, and its translocation to the nucleus (11–13). However, the precise molecular mechanisms associated with this process are obscure.

Several growth factors, including hepatocyte growth factor, transforming growth factor-β, vascular endothelial growth factor, and epidermal growth factor, have been reported to induce EMT in tumor cell lines (14–16). We have shown that the expression of CT and its G protein-coupled receptor (CTR) is remarkably higher in advanced PCs, and the CT-CTR autocrine axis is a potent stimulator of PC cell tumorigenicity, invasion, and metastasis (4, 17–19). Although CT-stimulated increase in the motility and invasion of PC cells may be mediated by CT-stimulated secretion of matrix metalloproteinases and urokinase-type plasminogen activator, the precise molecular mechanisms preceding these CTR actions remain to be elucidated (18, 20). We tested the hypothesis that CT induces biochemical and morphological changes associated with EMT to increase the invasiveness of PC cells.

Our results indicate that activation of the CT-CTR autocrine axis in prostate cancer cells induced several changes associated with EMT such as remodeling of tight and adherens junctions, cadherin switching, and activation of WNT/β-catenin signaling. In contrast, the silencing of the CT-CTR axis reversed this process. Moreover, cyclic AMP-dependent protein kinase (PKA) plays a key role in this CT-CTR-mediated process. This is the first study demonstrating the action of prostate CTR on junctional complexes and WNT/β-catenin signaling of PC cell lines.

* This work was supported, in whole or in part, by National Institutes of Health Grant CA96534 (to G. V. S.). The costs of publication of this article were defrayed in part by the payment of page charges. This article must therefore be hereby marked "*advertisement*" in accordance with 18 U.S.C. Section 1734 solely to indicate this fact.

[S] The on-line version of this article (available at http://www.jbc.org) contains supplemental Figs. 1 and 2 and Table 1.

[1] To whom correspondence should be addressed: 700 University Ave., Monroe, LA 71209. Fax: 318-342-1737; E-mail: shah@ulm.edu.

[2] The abbreviations used are: PC, prostate cancer; CT, calcitonin; CTR, CT receptor; EMT, epithelial-to-mesenchymal transition; PKA, cyclic AMP-dependent protein kinase; TRITC, tetramethylrhodamine isothiocyanate; ANOVA, analysis of variance; DAPI, 4′,6-diamidino-2-phenylindole; siRNA, short interfering RNA; TER, transepithelial resistance; TJ, tight junction; AJ, adherens junction; m-PKI, membrane-permeable, specific PKA inhibitor; ZO-1, zonula occludens-1; SV, vector expressing scrambled siRNA; APC, adenomatous polyposis coli; TCF, T cell factor.

EXPERIMENTAL PROCEDURES

Reagents and Antibodies—Hygromycin (Sigma), FuGENE 6 (Roche Applied Science), and TRITC-dextran 4000 (Sigma) were obtained from respective suppliers. Rabbit anti-zonula occludens (ZO-1) serum was purchased from Zymed Laboratories Inc.. Mouse anti-E-cadherin serum and rabbit anti-N-cadherin serum were obtained from Abcam (Cambridge, UK). Rabbit anti-β-catenin serum was purchased from Sigma. Horseradish peroxidase-conjugated anti-rabbit and anti-mouse IgG secondary antisera were from Promega (Madison, WI), and DAPI was purchased from Molecular Probes (Carlsbad, CA).

Reporter Plasmid Constructs—Luciferase-based reporters, pGL3-OT and pGL3-OF, were provided by Dr. Bert Vogelstein (Johns Hopkins University Medical Center).

Cell Culture—Highly metastatic PC-3M prostate cancer cell line was provided by Dr. Isaiah Fidler (MD Anderson Cancer Center, Houston, TX). The cells were maintained in complete medium (RPMI 1640 medium supplemented with 10% fetal bovine serum, 100 IU/ml penicillin G, and 100 μg/ml streptomycin) under standard culture conditions. Androgen-refractory PC-3 and androgen-responsive LNCaP cells were obtained from ATCC (Manassas, VA) and cultured as recommended by the ATCC (21, 22). PC-31 subline, isolated as the slower growing orthologue of PC-3 cells, lacked endogenous CT/CTR expression.

Activation or Inactivation of CT-CTR Autocrine Axis in PC Cell Lines by Stable Transfection—LNCaP cells express CTR but lack CT expression (4). In contrast, PC-3 cells express CT but lack endogenous CTR (4). The CT-CTR axis in these cell lines was activated by stable transfection of constitutively active vector (pcDNA3.1) containing either full-length CT cDNA insert (cloned from PC-3M cells) or full-length CTR cDNA (cloned from LNCaP cells). The resulting stable cell lines with the activated CT-CTR axis are referred as LNCaP-CT and PC-3-CTR, respectively. The control cell lines (referred to as LNCaP-V and PC-3-V) received carrier pcDNA 3.1 plasmid. PC-3M cells have an activated CT-CTR axis as they co-express CT and CTR (4). We inactivated this by stable transfection of either hammerhead ribozymes against CT mRNA or a plasmid pRNA-H1.1/Hygro (Genescript, Piscataway, NJ) containing previously validated siRNA duplexes against CTR mRNA (17, 23). The resulting PC-3M-CT$^-$ and PC-3M-CTR$^-$ cells displayed greater than 90% decrease in the abundance of endogenous CT or CTR mRNA as compared with their vector controls (PC-3M-V). The sublines were extensively characterized for CT or CTR expression as well as oncogenicity in recently published studies (17, 19, 23) (supplemental Fig. 1). The control PC-3M-V cell lines expressed either inactive ribozyme or the carrier plasmid prna-H.1/Hygro carrying scrambled siRNA duplexes of similar size, respectively. The expression of CT and/or CTR in PC-3M-V cells was not significantly different from parental PC-3M cells (17).

Formation of Acinar Structures by PC Sublines in Three-dimensional Collagen Gel—It has been shown that prostate cells and PC cell lines such as LNCaP organize to form spherical, cyst-like structures with lumen when cultured in collagen under previously defined three-dimensional culture conditions (24). To test the effect of activated CT-CTR axis on acinus formation by PC cells in three-dimensional culture, 5000 cells of each subline were plated on a collagen layer in acinus medium (RPMI 1640 complete medium containing 5% collagen, 10 ng/ml epidermal growth factor, 10 nM dihydrotestosterone). The collagen-coated chambers were then transferred to 37 °C 95% air, 5% CO_2 incubator. The medium was replaced every 4 days. Acinus formations started to form by day 8 and were photographed using Nikon TE-2000 microscope, and digital images were captured on a G4 Power PC computer by a Retiga 2300^{TM} monochrome digital camera using IPLab^{TM} image analysis program (Scanalytics Inc.).

Cell Compaction and Phase Contrast Microscopy—Approximately 2×10^4 cells per subline were plated in individual well of an 8-well chamber slide (Lab-Tek, Rochester, NY). Subconfluent colonies of the cells were observed daily using phase contrast Nikon-TE 2000 microscope, and their digital images were captured on a G4 Power PC computer by a Retiga 2300^{TM} monochrome digital camera using IPLab^{TM} image analysis program (Scanalytics Inc., Rockville, MD). The distance between cells (at least 20 cells/×400 field and five fields per subline) was measured.

Preparation of Cell Lysates, Triton X-100-soluble and -insoluble Fractions—Confluent 100-mm plates of each PC subline were serum-starved overnight and treated with/without 50 nM CT for periods as described under "Results." Triton X-100-soluble extract (cytosolic) was obtained by incubating cells with 10 mM Tris-HCl, pH 7.4 (containing 150 mM NaCl, 2 mM $CaCl_2$, 1 mM phenylmethylsulfonyl fluoride, 40 units/ml aprotinin, 15 μg/ml leupeptin, 1% Nonidet P-40, and 1% Triton X-100), for 30 min with occasional agitation. After washing the plates with Tris-buffered saline (containing protease inhibitors), the Triton X-100-insoluble fraction (plasma membrane-associated) was scraped out from the plates with Tris-buffered saline containing 0.5% SDS, 1% Nonidet P-40, 40 units/ml aprotinin, and 15 μg/ml leupeptin. The Triton X-100-insoluble fraction was collected after homogenizing and centrifuging at 14,000 × *g* for 5 min at 4 °C, and the protein content of the supernatants was determined using Bio-Rad reagent.

Nuclear Fraction—Several 100-mm plates (~8×10^6 cells per plate) of serum-starved cells were treated with 50 nM CT for 0, 1, 4, and 8 h. The cells were washed with ice-cold Ca^{2+}/Mg^{2+}-free phosphate-buffered saline and lysed in a lysis buffer (10 mM HEPES, pH 7.9, 1.5 mM $MgCl_2$, 10 mM KCl, 1 mM dithiothreitol, 1 mM phenylmethylsulfonyl fluoride). The lysate was then homogenized using a Dounce homogenizer. After incubation on ice for 10 min, lysate was centrifuged at 850 × *g* for 10 min at 4 °C. The pellet was resuspended in ice-cold lysis buffer containing 1% Triton X-100 and recentrifuged at 850 × *g* for 10 min at 4 °C. The crude nuclear pellet was resuspended in 100 μl of buffer (20 mM HEPES, pH 7.9, 25% glycerol (v/v), 0.42 M NaCl, 1.5 mM $MgCl_2$, 0.2 mM EDTA, 0.5 mM dithiothreitol, 1 mM phenylmethylsulfonyl fluoride). Nuclear proteins were recovered after centrifugation at 20,000 × *g* for 15 min at 4 °C, and the protein content of the supernatants was determined using Bio-Rad reagent.

Western Blotting—The lysate fractions were boiled for 5 min in 2× Laemmli solution containing 20 mM dithiothreitol, and 50 μg of protein was loaded per lane of 10% SDS-polyacrylamide gel, and fractionated proteins were electrically transferred to a nitrocellulose membrane. The blots were incubated with appropriate antisera as described under "Results" for 18 h at 4 °C, followed by appropriate horseradish peroxidase-conjugated secondary antisera. The immune complexes were visualized on chemiluminescence radiography film using Western blot ECL detection system (Radiochemical Center, Amersham Biosciences). The blots were then washed and reprobed for α-tubulin. The same experiment was repeated two more times. The density of the bands was semi-quantitatively estimated by densitometry.

Reporter Assays—PC cells were plated at a subconfluent density (10^5 cells/35-mm dish) and co-transfected with 1 μg of the appropriate reporter (pGL3-OT or pGL3-OF) and 0.1 μg of pRL-TK using FuGENE 6 (Roche Applied Science). After serum starvation for 24 h, the cells were stimulated with CT in serum-free medium and lysed at the desired times. The reporter activity was measured using dual luciferase assay according to the manufacturer's instructions (Promega). To correct for potential variations in transfection or lysis efficiency, luciferase signals were normalized with *Renilla* luciferase signal.

WNT Signaling Pathway Gene Array—Total RNA of vehicle or CT (50 nM)-treated PC-31-CTR cells (CT^-/CTR^+; CTR expression in PC-31 cells was enforced by stable transfection of pcDNA3.1-CTR plasmid) was isolated using TRIzol™ according to the manufacturer (Invitrogen). The RNA was further purified using isopropyl alcohol precipitation and was concentrated using the RNeasy MiniElute cleanup kit (Qiagen). The quantity of total RNA was measured, and the RNA quality was examined with Agilent 2100 bioanalyzer (Agilent Technologies). Total RNA (3 μg) was used for cDNA synthesis, labeling, and amplification. The labeled cDNA was hybridized to a WNT signaling pathway Oligo GEArray membrane (OHS-043) according to the manufacturer's protocol (SuperArray). After chemiluminescent detection, images were analyzed using manufacturer's software (SuperArray).

Measurement of Transepithelial Resistance (TER)—Approximately 1×10^5 cells were plated and grown to confluency on 12-well Transwell filters (0.4 μm pore size) in complete medium for first 12 h and then in serum-free medium. TER was measured in triplicate wells using EVOM volt-ohm meter (World Precision Instruments, Sarasota, FL) before and at multiple time points after CT addition. The TER values were normalized to the area of the monolayer filter, and calculated by subtracting the blank values derived from the filters containing only bathing medium.

Paracellular Permeability (Paracellular Diffusion of Dextran)—Approximately 1×10^5 cells were plated and grown to confluency on 12-well Transwell filters in complete medium. Tetramethylrhodamine-dextran (an average molecular mass of 4 kDa; Sigma), dissolved in Hanks' balanced salt solution to a concentration of 1 mg/ml, was added to the upper chamber. The lower chamber was replaced with Hanks' balanced salt solution. After incubating for 1 h at 37 °C, 100-μl aliquots were collected from the lower chamber and assayed for fluorescence using spectrophotometer at 530 nm excitation/590 nm emission.

Immunofluorescence of Junction Proteins—Approximately 1×10^5 PC-31-CTR cells were plated at confluency and grown on 0.4-μm 12-well Transwell filters (Costar, MA) in complete medium for 4 days for optimal tight junction (TJ) development. After overnight serum starvation, cells were treated with/without 50 nM CT for 60 min and then fixed with methanol for 10 min at −20 °C. The cells were incubated with either rabbit anti-ZO-1 IgG (Zymed Laboratories Inc.), β-catenin (Cell Signaling), or mouse monoclonal E-cadherin (Abcam, Cambridge, UK) in blocking solution (phosphate-buffered saline, 0.3% Triton X-100, 10% goat serum) overnight at 4 °C. Staining was visualized after incubation with goat anti-rabbit TRITC (1:500) for 1 h in the dark at room temperature. Controls with either nonimmune goat IgG or no primary antisera were used in all studies. Digital photographs were taken with Retiga 1300 camera connected to a Nikon Optiphot-2 microscope equipped for epifluorescence, and the images were captured at different wavelengths for TRITC and DAPI, were given red and blue pseudo colors, respectively, and were analyzed using IP Lab™ image analysis program.

Immunofluorescence of Tumor Xenografts—We have demonstrated that the modulation of the CT-CTR axis in PC cell lines significantly alters their growth and tumor formation in nude mice (17, 25). We used paraformaldehyde-fixed, paraffin-embedded tumor xenografts of earlier studies to examine the effect of CT-CTR axis modulation on immunoreactivity of E- and N-cadherins in tumor xenografts *in vivo* (17, 25). The 5-μm-thick sections of tumor xenografts were deparaffinized, hydrated, and processed for E- and N-cadherin using mouse anti-E-cadherin and rabbit anti-N-cadherin sera (Abcam, Cambridge, UK). Staining was visualized with appropriate TRITC-conjugated secondary antisera (1:500). The sections were then counterstained with DAPI (1:45,000; Molecular Probes) for 10 min at room temperature.

Digital images of high power field (×400) taken by Nikon Optiphot-2 microscope were captured on a G4 Power PC computer by a Retiga 2300™ monochrome digital camera using IPLab™ image analysis program (Scanalytics Inc.). The images for each field were captured in two colors (red and blue) separately. Ten random images per section were obtained. The percentage of a specific antigen-positive cells in each specimen was also determined by counting immunopositive and total cells in at least 10 ×400 fields per specimen.

Statistical Analysis—The results were statistically evaluated by One-way ANOVA analysis, and the levels of significance were derived from Newman-Keuls test. The difference was considered statistically significant when $p < 0.05$.

RESULTS

Activation of CT-CTR Autocrine Axis Alters Cell-Cell Compaction Pattern of PC Cells—Poorly differentiated PCs often display elevated co-expression of CT and CTR (4). Because exogenously added CT also increases the invasion of CTR-positive PC cell lines (18), we tested the hypothesis that activation of CT-CTR autocrine loop alters cell-cell adhesion (9). We acti-

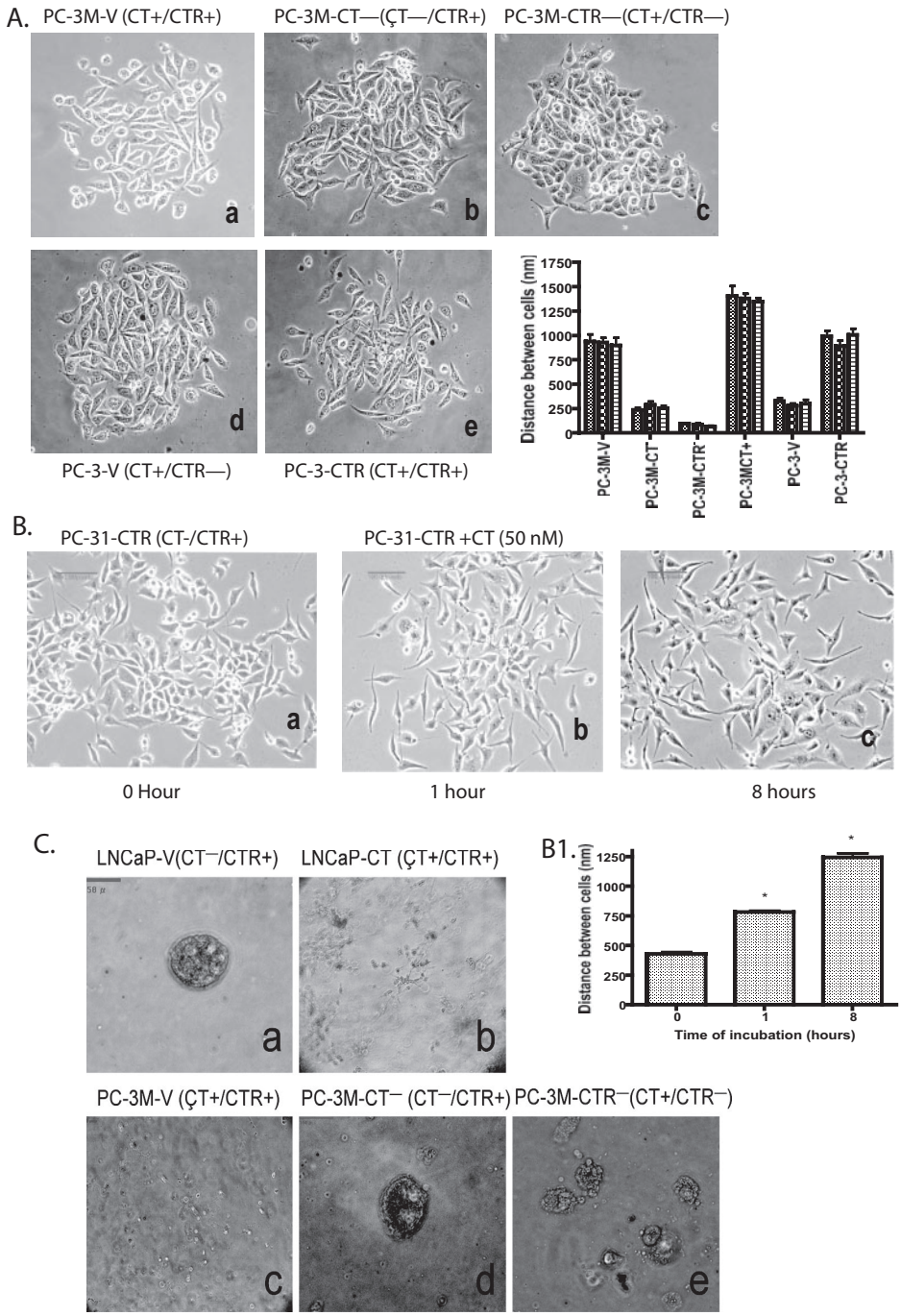

FIGURE 1. **CT-CTR axis and cell-cell adhesion.** *A,* phase contrast micrographs (×100) of subconfluent PC lines show changes in cell-cell compaction pattern caused by modulation of CT/CTR expression. *Panel a,* empty vector transfected PC-3M cells (PC-3M-V); *panel b,* CT down-regulated PC-3M cells (PC-3M-CT$^-$); *panel c,* CTR down-regulated PC-3M cells (PC-3M-CTR$^-$); *panel d,* PC-3 cells transfected with empty vector (PC-3-V); *panel e,* PC-3 cells with enforced CTR (PC-3-CTR); *panel f,* distance between cells of three different clones of each cell lines in *a–e* is expressed as nm ± S.E. for $n = 20$. *, $p < 0.001$; two-way ANOVA (active CT-CTR axis *versus* inactive CT-CTR axis). *B,* phase contrast micrographs (×100) of subconfluent cultures of PC-31-CTR cells treated acutely with 50 nM CT for different time periods. PC-3-CTR cell cultures were photographed after treatment with 50 nM for *panel a,* 0 min; *panel b,* 1 h; and *panel c,* 8 h. *B1* presents the mean inter-cell distance nm ± S.E. at each time point for $n = 36$. *, $p < 0.005$; one-way ANOVA and Newman-Keuls test. *C,* PC cells were seeded on collagen in acinus medium as described under "Experimental Procedures." Phase contrast images (×100) of acinar structures were captured on the 14th day. *Panel a,* LNCaP vector controls (LNCaP-V); *panel b,* LNCaP cells with enforced CT expression (LNCaP-CT); *panel c,* PC-3M vector controls (PC-3M-V); *panel d,* CT down-regulated PC-3M cells (PC-3M-CT$^-$); *panel e,* CTR down-regulated PC-3M cells (PC-3M-CTR$^-$).

vated CT-CTR axis in PC-3 cells by enforcing the expression of CTR (PC-3-CTR). In contrast, we silenced CT-CTR axis in PC-3M cells with knockdown of CT or CTR (PC-3M-CT$^-$ or PC-3M-CTR$^-$) (17). We then examined the compaction profile of these sublines in two-dimensional culture by phase contrast microscopy (Fig. 1).

PC-3M-V (vector control, CT$^+$/CTR$^+$) cells formed discrete colonies. However, the cells also displayed separation from neighboring cells (mean distance between cells: 920 nm ± 38.87, $n = 50$) (Fig. 1*A, panel a*). The loss of either CT (PC-3M-CT$^-$) or CTR (PC-3M-CTR$^-$) expression remarkably increased cell-cell compaction (Fig. 1*A, panels b* and *c*). Both, PC-3M-CT$^-$ and PC-3M-CTR$^-$ cells grew in larger colonies with typical epithelial, cobblestone-like appearance (mean inter-cell distance: 255 ± 17 nm for CT$^-$ cells; 79 ± 8 nm for CTR$^-$ cells). The loss of CTR produced more prominent changes than those produced by CT knockdown. PC-3-V cells (vector control, CT$^+$/CTR$^-$) also formed discrete colonies, and the cells were more compact than PC-3M-V (CT$^+$/CTR$^+$) cells (mean intercell distance: PC-3-V cells, 303 ± 20 nm ($n = 50$) *versus* 920 ± 39 nm for PC-3M-V cells ($n = 50$); Fig. 1*A, panel a versus d*). Enforced CTR expression in PC-3 cells (PC-3-CTR; CT$^+$/CTR$^+$) led to increased scattering (mean intercell distance: 968 ± 36 nm, $n = 50$; Fig. 1*A, panel e*). Fig. 1*A, panel f,* depicts mean inter-cell distance ± S.E. in three separate clones of each cell line ($n = 24$). The results demonstrate that individual clones of all cell lines displayed similar cell-cell compaction, and the cell lines with inactive CT-CTR axis (PC-3-V, PC-3M-CT$^-$, and PC-3M-CTR$^-$) displayed remarkably greater cell-cell compaction than the cell lines with active CT-CTR axis (PC-3M-V, PC-3M-CT$^+$, and PC-3-CTR).

We also examined acute effects of exogenously added CT on compaction pattern of PC-31-CTR (CT$^-$/CTR$^+$) cells. These cells do not synthesize CT but are responsive to CT because of enforced CTR expression. As depicted in Fig. 1*B*, the cells displayed cuboidal shape. Treatment with 50 nM CT led to scattering of cells within 1 h, which increased remarkably after

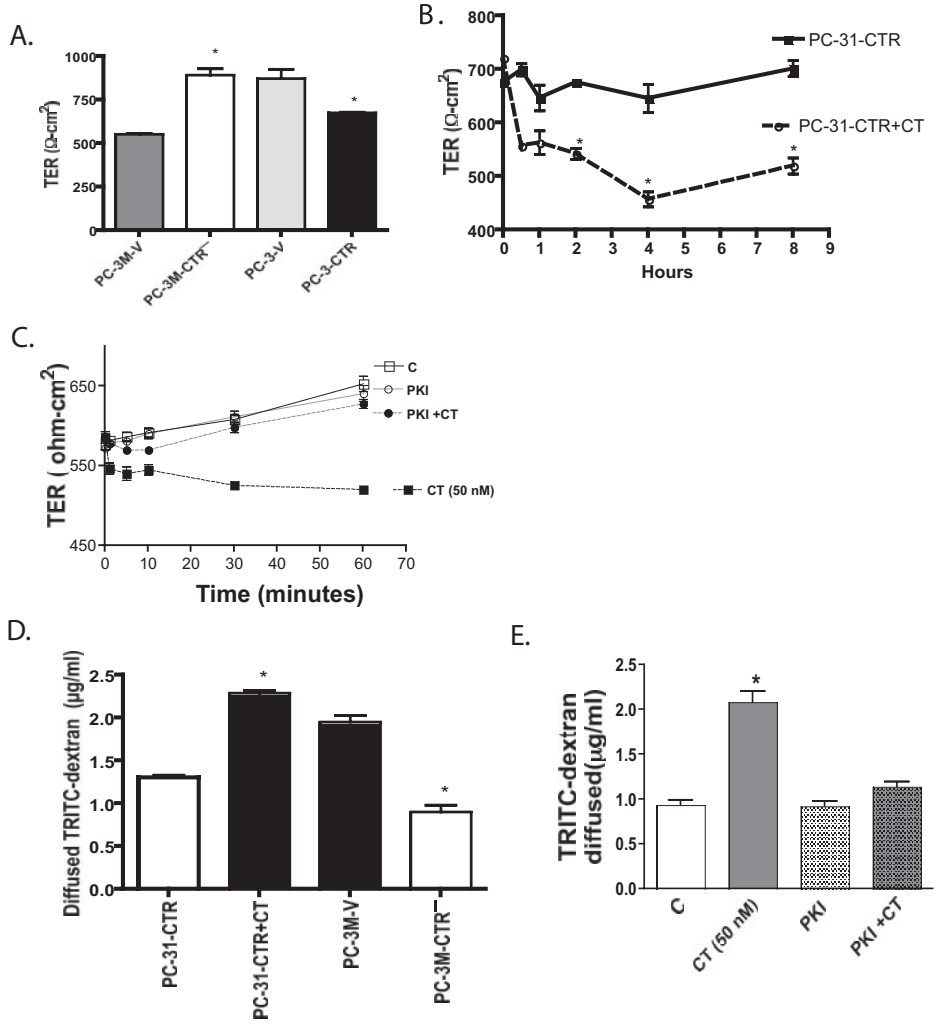

FIGURE 2. **Effect of CT-CTR axis on TER and paracellular permeability.** *A,* monolayers of PC-3M-V, PC-3M-CTR$^-$, PC-3-V, and PC-3-CTR cells were allowed to polarize, and TER values were measured 3 days after plating. Results are mean TER ± S.E. ($n = 3$). Data were compiled from three separate experiments. *, $p < 0.05$ significantly different from their respective controls (one-way ANOVA and Newman-Keuls test). *B,* monolayer cultures of PC-31-CTR cells were exposed to 50 nM CT 24 h after plating. TER values were measured from 5 min to 8 h after CT treatments. Results are mean TER ± S.E. ($n = 3$) normalized to control monolayers of PC-31-CTR cells at each time point. Data were compiled from three separate experiments. *, $p < 0.05$ significantly different from their respective controls (one-way ANOVA and Newman-Keuls test). *C,* polarized PC-31-CTR cells on transwells were treated with vehicle, CT (50 nM), m-PKI (100 nM), or m-PKI+CT. Their TER was measured at several time points after the addition of agents. *D,* polarized monolayer cultures of PC-3M-V, PC-3M-CTR$^-$, PC-31-CTR, and PC-31-CTR cells treated with 50 nM CT for 4 h. The cells were then treated with TRITC-dextran (500 μl of 1 mg/ml solution) in the upper chamber. After 1 h, 100 μl of media was drawn from the lower chamber and assayed for fluorescence using spectrophotometer at 530 nm excitation and 590 nm emission. *, $p < 0.05$ significantly different from their respective controls (one-way ANOVA and Newman-Keuls test). *E,* polarized PC-31-CTR cells on transwells were treated with vehicle, CT (50 nM), m-PKI (100 nM), or m-PKI+CT. Their paracellular permeability was determined by diffusion of TRITC-dextran after 1 h incubation with the agents. The results are expressed as mean ± S.E. ($n = 4$). *, $p < 0.05$ significantly different from control (one-way ANOVA and Newman-Keuls test).

8 h (Fig. 1, *B* and *B1*). Each field was pictured at same magnification, and the apparent decrease in cell number with increased time of incubation was because of cell migration and not apoptosis (26).

Formation of Acinus Structures in Three-dimensional Cell Culture—LNCaP prostate cancer cells form acini-like structures when cultured in three-dimensional collagen gel under specific conditions (24, 27). We used this model to examine the effect of the CT-CTR axis on acinus-forming ability of LNCaP (CT$^-$/CTR$^+$) and PC-3M (CT$^+$/CTR$^+$) sublines. As depicted in Fig. 1*C, panel a,* LNCaP-V cells clustered to form acinar structures with lumen-like space after 8 days in three-dimensional culture. However, LNCaP cells lost the ability to form acini when CT expression was enforced (Fig. 1*C, panel b*), suggesting that the activation with the CT-CTR axis prevents the formation of acinar structures. PC-3M-V (CT$^+$/CTR$^+$) cells did not cluster to form multicellular structures (Fig. 1*C, panel c*). However, the knockdown of either CT or CTR enabled them to form such structures (Fig. 1*C, panels d and e*). Because cell-cell junctions are critical for this process, we next examined the effect of CT-CTR axis on tight (TJ) and adherens junctions (AJ) of PC cell lines.

Activation of CT-CTR Axis and Cell-Cell Junctions—TJ is an occluding seal between the neighboring cells that is located at the most apical part of their lateral membranes (28, 29). The paracellular space in the TJ is completely obliterated after each strand associates laterally with a strand of an adjacent cell to form "paired" strands, generating a primary barrier to the flux of fluid, electrolytes, and macromolecules. We examined TJs in PC sublines by measuring TER and paracellular permeability of polarized, confluent PC cell cultures. Polarized cells with active CT-CTR axis such as PC-3M-V and PC-3-CTR displayed significantly lower TER than those that lack CTR such as PC-3-V or PC-3M-CTR$^-$ cells, raising a possibility that the activation of CTR may destabilize TJs resulting in a leaky cell layer (Fig. 2*A*). To examine the acute effect of the CT-CTR axis on TER, we stimulated PC-31-CTR cells with 50 nM and examined TER over a period of time. Unstimulated PC-31-CTR cells displayed fairly stable TER over a period of 8 h (Fig. 2*B*). However, the addition of CT caused a rapid TER decline from 720 ± 5.3 to 557 ± 6.02 within 30 min, and further to 457 ± 13.8 in 4 h. Because CTR is coupled to $G\alpha_s$ and activates cyclic AMP-dependent protein kinase (PKA) (30), we next examined whether m-PKI, a membrane-permeable, specific PKA inhibitor, reverses the actions of CT on TER. 100 nM m-PKI did not affect TER of PC-31-CTR cells by itself but completely abolished the actions of CT on TER (Fig. 2*C*).

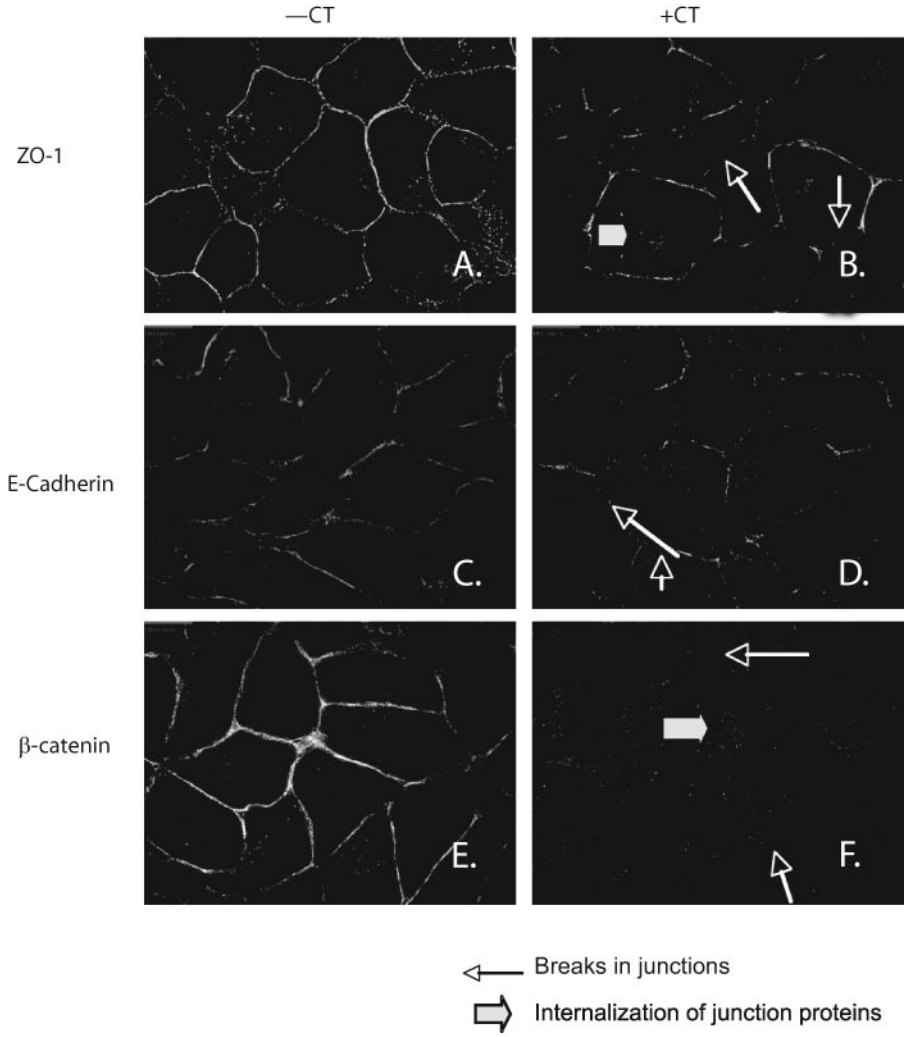

FIGURE 3. **Localization of junctional proteins by immunofluorescence.** Confluent monolayer of PC-31-CTR cells grown on Transwell filters were allowed to polarize for 4 days. The cells were then treated with 50 nM CT for 60 min and fixed with methanol at −20 °C for 10 min. After immunofluorescent staining for ZO-1, E-cadherin, and β-catenin, ×400 pictures were captured. The focus was adjusted to the basolateral plane. *Left panels* present vehicle-treated cells; and *right panels* present cells treated with CT.

The TJs of polarized cell sheet form a tight barrier so that inert material such as dextran cannot pass through it. We examined barrier function of TJs in PC cell cultures by testing the permeability of TRITC-dextran (average mass of 4 kDa) through the cell layer. If CT-CTR axis destabilizes TJs, the barrier should become porous enabling more dextran to pass through the cell layer. The results of Fig. 2*D* show that the cells with inactive CT-CTR axis (PC-3M-CTR$^-$ and PC-31-CTR) displayed remarkably lower paracellular permeability than cells with activated CT-CTR axis (PC-31-CTR+CT and PC-3M-V cells). Once again, the knockdown of CTR in PC-3M cells led to a marked decline in their paracellular permeability from 1.951 ± 0.075 to 0.903 ± 0.079. We examined the role of PKA in this process by testing whether m-PKI reverses the actions of CT on paracellular permeability of PC-31-CTR cells. Once again, mPKI did not affect paracellular permeability of PC-31-CTR cells but abolished the actions of CT on paracellular permeability (Fig. 2*E*). These results again suggest that the destabilizing actions of CT on TJs in PC cell lines are PKA-mediated.

Effect of CT-CTR Axis on TJs and AJs, Localization of Junctional Proteins by Immunofluorescence—Integrity of TJ and AJ can also be examined by immunolocalization of key junction proteins such as ZO-1 (for TJs) and E-cadherin/β-catenin (for AJs) in polarized cells (31). The location of these proteins along complete cell borders is suggestive of intact junctions. However, breaks or thinning of these borders and intracellular staining of membrane proteins suggest disruption of junctions. We examined the acute effect of CT on the location of ZO-1, E-cadherin, and β-catenin in polarized PC-31-CTR cells by immunofluorescence. These proteins were localized along cell perimeter in unstimulated PC-31-CTR cells (Fig. 3, *A, C,* and *E*). However, CTR activation delocalized these proteins within 60 min as suggested by broken cell borders and intracellular staining of ZO-1 and β-catenin (Fig. 3, *B, D,* and *F*).

CT Induces EMT of PC Cells—Because the results of Fig. 3 indicate that CT stimulated disassembly/remodeling of junctions and internalization of integral membrane proteins, we sought to confirm this by investigating the effect of CT on Triton X-100 solubility of key junction proteins. This is because proteins localized in plasma membrane are Triton X-100-insoluble and become soluble in Triton X-100 with their translocation into cytoplasm (32). Triton X-100-insoluble and -soluble fractions of cell lysates were loaded onto SDS-PAGE and immunoblotted for ZO-1, E-cadherin, N-cadherin, and β-catenin. α-Tubulin and β-actin were respective loading controls. The bands were then quantitated by densitometry, and each membrane protein was normalized to its loading control. The data are expressed either as the ratio of proteins in Triton X-100-soluble fraction/Triton X-100-insoluble fraction or as N-cadherin/E-cadherin. Increase in the ratio of Triton X-100-soluble/Triton X-100-insoluble is suggestive of their translocation from the membrane into cytoplasm.

Activation of CT-CTR Axis Induces Internalization of ZO-1 and β-Catenin—The results of Fig. 4 suggest that the inactivation of the CT-CTR axis in PC-3M cells (knockdown of CTR) led to a remarkable decrease in cytoplasmic ZO-1 levels (Fig. 4*B, lanes 1–3*). Densitometric quantitation of the blots revealed a remarkable decrease in soluble/insoluble ratio, suggesting that the inactivation of CT-CTR axis in PC-3M cells caused the translocation of ZO-1 to the mem-

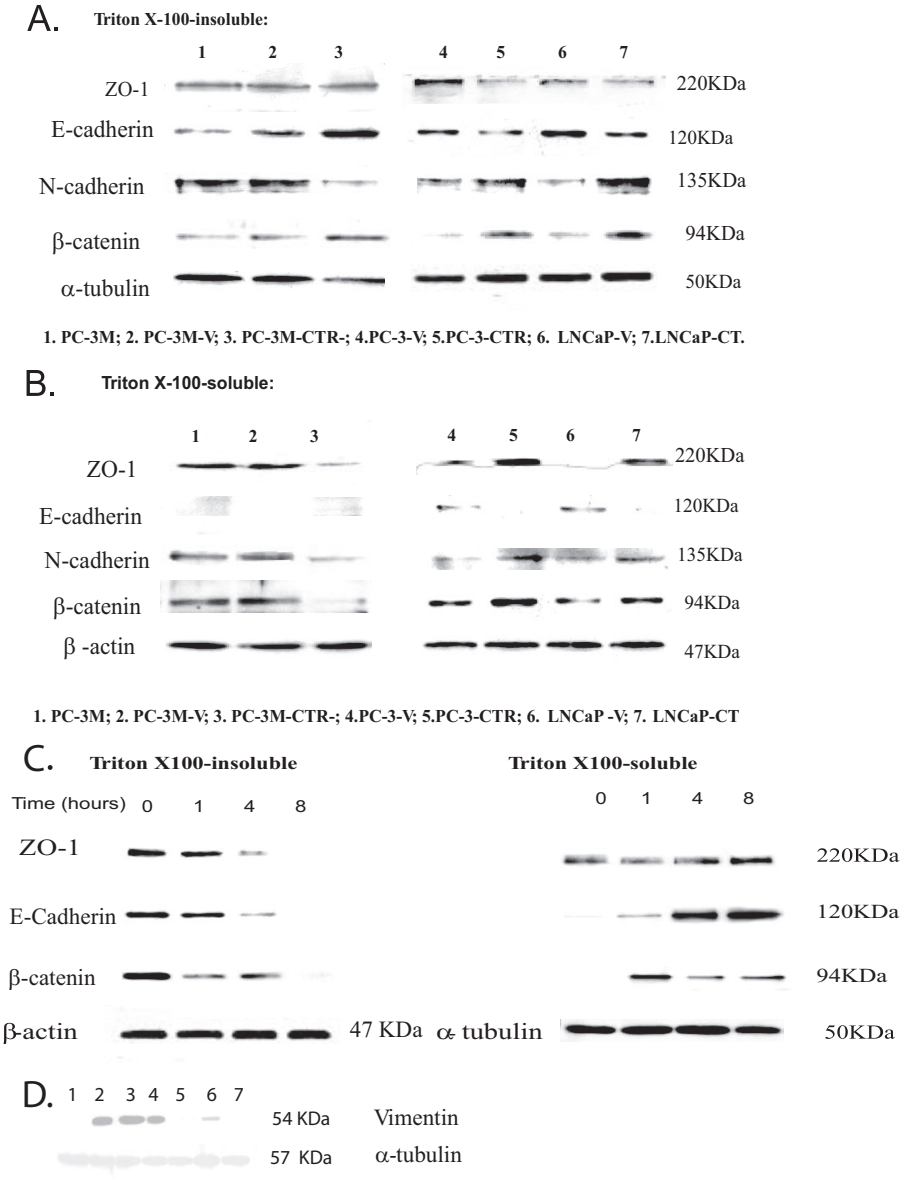

FIGURE 4. **Localization of junctional proteins, immunoblotting.** Confluent monolayers of PC sublines were lysed with cytosolic lysis buffer for 30 min to collect Triton X-100-soluble fraction. Then the cells were lysed in membrane lysis buffer to obtain Triton X-100-insoluble fraction. Western blot analysis for ZO-1, E-cadherin, N-cadherin, and β-catenin was carried out after loading 40 μg of Triton X-100-soluble proteins and 20 μg of Triton X-100-insoluble proteins. β-Actin and α-tubulin were respective loading controls. The experiment was repeated three separate times. *A,* Western blot of junction proteins in Triton X-100-insoluble fraction. *B,* Western blot of junction proteins in Triton X-100-soluble fraction. *C,* Western blot of junction proteins in Triton X-100-insoluble and Triton X-100-souble fractions after acute stimulation of PC-31 cells with CT. Confluent monolayers of PC-31-CTR cell were serum-starved and treated with 50 nM CT for periods of 1, 4, and 8 h. Cells were first treated with cytosolic lysis buffer for 30 min to collect cytosolic fraction. Then the cells were lysed in membrane lysis buffer. Western blot analysis for ZO-1, E-cadherin, and β-catenin was carried out after loading 40 μg of cytosolic proteins and 20 μg of membrane proteins. α-Tubulin and β-actin were respective loading controls. The experiment was repeated three separate times. *D,* Western blot of vimentin immunoreactivity in PC cell lines. Confluent monolayers of PC sublines were lysed and subjected to SDS-PAGE and Western blot analysis as described under "Experimental Procedures" after loading 80 μg of lysate proteins. α-Tubulin was the loading control. The experiment was repeated three separate times. *Lane 1,* LNCaP; *lane 2,* PC-3-CTR; *lane 3,* PC-3M; *lane 4,* PC-3M-CT$^+$; *lane 5,* PC-3M-CTR$^-$; *lane 6,* PC-3; *lane 7,* PC-3M-CT$^-$.

brane (Fig. 5*A*). In contrast, activation of CT-CTR axis in PC-3 and LNCaP cells increased the ratio, suggesting internalization of ZO-1 to the cytosol (Fig. 4, *A* and *B*, *lanes 4–7*; Fig. 5*A*). β-Catenin also followed a similar pattern (Fig. 4, *A* and *B*; Fig. 5*A*). Acute activation of CTR also caused internalization of ZO-1 and β-catenin as characterized by a marked decline of these proteins in Triton X-100-insoluble fraction with a concomitant increase in Triton X-100-soluble fraction (Fig. 4*C*).

Activation of CT-CTR Axis Induces Cadherin Switch—We also compared relative distribution of N- and E-cadherin in these cell lines. This is because cadherin switching (increase in N-cadherin with concomitant decrease in E-cadherin) is associated with the induction of EMT, a process crucial for the progression of localized tumor into a metastatic one (13). If CT-CTR axis induces EMT, then its activation should increase the N-cadherin/E-cadherin ratio. The results of Figs. 4 and 5 demonstrate that the knockdown of CTR in PC-3M cells increased the levels of E-cadherin (from 0.948 ± 0.067 to 2.837 ± 0.449), and decreased the levels of N-cadherin (1.013 ± 0.005 to 0.306 ± 0.014) in Triton X-100-insoluble fraction (Fig. 4*A, lanes 1–3*; Fig. 5*B*). In contrast, the activation of the CT-CTR axis in PC-3 and LNCaP cells led to an approximate 3-fold decrease in the levels of E-cadherin in Triton X-100-insoluble fractions with a corresponding 2–3-fold increase in the levels of N-cadherin and β-catenin (Fig. 4*A, lanes 4–7*; Fig. 5*B*). These proteins also displayed a similar profile in Triton X-100-soluble fractions (Fig. 4*B, lanes 4–7*; Fig. 5*B*).

To confirm that CT-CTR axis-induced cadherin switch is associated EMT, we examined the levels of vimentin, a mesenchymal marker (33). The results of Fig. 4*D* are consistent with those of Fig. 4, *A* and *B,* and suggest that the cells with active CT-CTR axis (PC-3M, PC-3M-CT$^+$, and PC-3-CTR) expressed high levels of vimentin (Fig. 4*D, lanes 2–4*). In contrast, the cells with inactive CT-CTR axis (LNCaP, PC-3M-CT$^-$, and PC-3M-CTR$^-$) had undetectable vimentin immunoreactivity (Fig. 4*D, lanes 1, 5,* and *7*). PC-3-V cells (with inactive CT-CTR axis) displayed detectable vimentin immunoreactivity, but still remarkably less than those with active CT-CTR axis (Fig. 4*D, lane 6*; Fig. 5*C*).

In Vivo Studies Confirm the Association between Active CT-CTR Axis and Cadherin Switch—Because the results of Fig. 4 suggest that the activation of CT-CTR axis induced the cad-

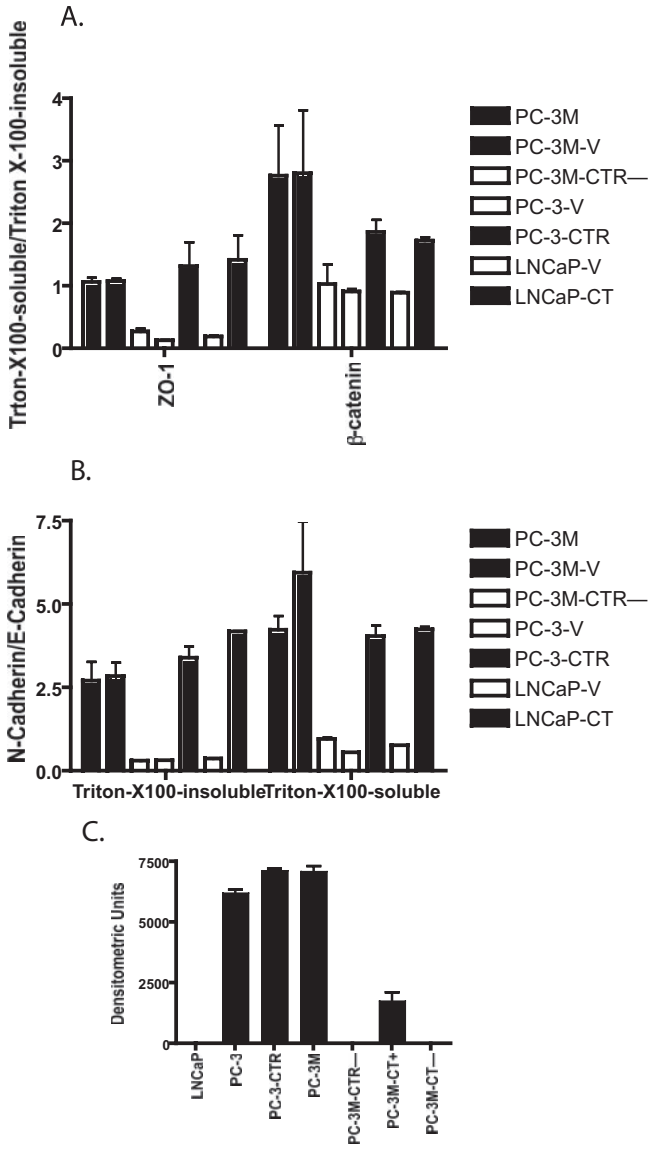

FIGURE 5. **Densitometric quantitation of blots of Fig. 4.** The developed immunoblots were scanned on a Bio-Rad densitometer. The data from three blots were pooled and presented as means ± S.E. for $n = 3$. *A,* quantitation of Western blots in Fig. 4, *A* and *B,* presented as a ratio of Triton X-100-soluble/Triton X-100-insoluble levels of ZO-1 and β-catenin. *B,* quantitation of Western blots in Fig. 4, *A* and *B,* presented as a ratio of N-cadherin/E-cadherin. *C,* quantitation of vimentin blots of Fig. 4*D*.

herin switch, we tested whether a similar phenomenon occurs *in vivo*. We examined the levels of immunoreactive E-cadherin and N-cadherin by immunofluorescence in two sets of xenografts generated in our earlier studies (17, 25). As depicted in Fig. 6*A*, PC-3M-V (CT^+/CTR^+) xenografts displayed extremely low number of E-cadherin-immunopositive cells (5%), and the majority of cells were positive for N-cadherin-immunopositive cells (75%). In contrast, PC-3M-CTR^- xenografts displayed a reverse profile as indicated by the higher number of E-cadherin-immunopositive cells (>75%), and remarkably lesser N-cadherin-immunopositive cells (<5%) (Fig. 6*B*). PC-3-V (CT^+/CTR^-) xenografts also displayed relatively higher percentage of E-cadherin-immunopositive cells (>70%) and a few N-cadherin-immunopositive cells (<5%). However, this pattern was reversed with enforced CTR expression (E-cadherin-positive ~12%, N-cadherin-positive >70%). These results reinforce an association between the activation of CT-CTR autocrine axis and cadherin switching.

In a recent study, we injected the plasmid expressing siRNA against CTR (CTR^-) intratumorally to knock down CTR expression after the initial growth of PC-3M (CT^+/CTR^+) xenografts. We have shown that this treatment knocked down CTR expression and markedly attenuated xenograft growth when compared with those receiving the plasmid expressing scrambled siRNA (SV) (25). We examined these paraffin-embedded tumors for E-cadherin and N-cadherin immunoreactivity. The results of Fig. 6*C* have shown that *in vivo* knockdown of CTR in preexisting PC-3M xenografts increased the number of E-cadherin-immunoreactive cells (from <5 to >80%) while decreasing the population of N-cadherin-immunoreactive cells (from >75 to ~5%) (SV *versus* CTR^-) (Fig. 6*D*). These results are consistent with our *in vitro* results and support a possibility that the activation of CT-CTR autocrine axis can induce EMT of prostate cancer cells, possibly by disassembly/remodeling of cell-cell junctions, cadherin switching, and internalization of ZO-1 and β-catenin.

CT Increases the Levels of Cytosolic and Nuclear β-Catenin—Because CTR activation led to the disassembly of AJs and internalization of β-catenin, we examined the fate of β-catenin in response to acute CT stimulation. Intracellular β-catenin is usually cleared by ubiquitination/proteasome degradation by APC-AXIN2-GSK3β complex (34). Disruption of this complex stabilizes intracellular β-catenin, leading to its translocation in the nucleus, where it can bind to its partner *LEF-1* (lymphocyte enhancer factor-1) to transactivate target genes (35). We first examined the location of β-catenin immunoreactivity in CT-treated PC-31-CTR cells by immunofluorescence at multiple time points (0–12 h). CT caused an increase in cytosolic β-catenin immunoreactivity relatively rapidly (within 30 min, data not shown). However, strong nuclear β-catenin immunoreactivity was observed only 8 h after CT stimulus (Fig. 7*A*). To confirm these results, we examined the levels of β-catenin in membrane-associated, cytosolic, and nuclear fractions of PC-31-CTR cells at several time points after CT (50 nM) stimulus. As shown in Fig. 7*B*, CT induced a time-dependent decrease in β-catenin immunoreactivity in the membrane-associated fraction. This was accompanied by a rapid increase of cytosolic β-catenin at 1 h after CT stimulation, which subsequently declined at 4 and 8 h. β-Catenin immunoreactivity in nuclear fraction was detected at 4 h after CT stimulus but was significantly greater at 8 h, confirming the results of immunofluorescence (Fig. 7*B*). The levels of β-actin or α-tubulin (loading controls for cytosolic/membrane fractions) were similar at all time points in both the cytosolic and membrane-associated fractions. Normalization of nuclear proteins was carried out with TATA-binding protein.

CT Stimulates β-Catenin-responsive Transcription—Nuclear β-catenin complexes with *LEF/TCF-4* to create a bipartite transcription complex that activates downstream EMT-promoting genes (35). Because CT increased the nuclear pool of β-catenin, we examined β-catenin-mediated transcriptional activity using luciferase-based reporter plasmids, pGL3-OT and pGL3-OF, the improved version of the Topflash and Fop-

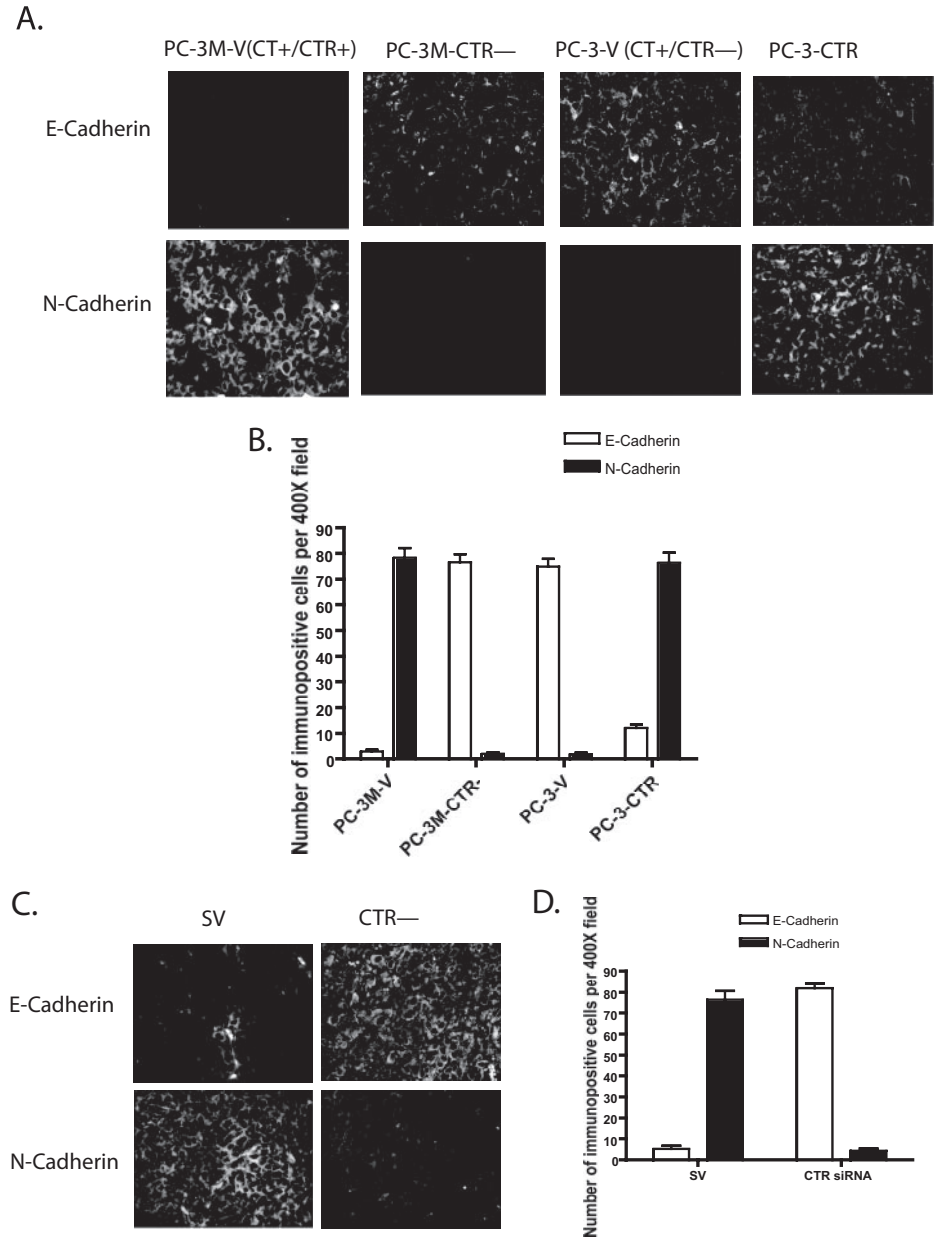

FIGURE 6. **Immunofluorescence of E- and N-cadherin in tumor xenografts.** E-cadherin- and N-cadherin-immunopositive cells in the tumor were identified by immunofluorescence in two sets of xenografts. *A,* xenografts of PC-3M-V, PC-3M-CTR$^-$, PC-3-V, and PC-3-CTR cell lines were probed for E-cadherin and N-cadherin immunoreactivity (4 sections/xenograft). Six ×400 micrographs (per each specimen) were captured from tumor xenografts of four different animals. *B,* number of immunopositive cells and total cells (DAPI-positive) in each micrograph were counted. The results are presented as mean ± S.E. ($n = 24$). *C,* mice bearing PC-3M xenografts were treated with the vector expressing either scrambled siRNA (SV) or CTR siRNA (CTR$^-$) as described in earlier studies (25). Four sections of each of these xenografts were probed for E-cadherin and N-cadherin immunoreactivity. Six ×400 micrographs were captured from tumor xenografts of four different animals. *D,* number of immunopositive cells and total cells (DAPI-positive) in each micrograph were counted. The results are presented as mean ± S.E. ($n = 24$).

flash vectors (36). The plasmid-transfected cells were kept in serum-free medium, and stimulated with various concentrations of CT (0–500 nM) for 8 h. CT promoted a dose-dependent increase in pGL3-OT luciferase, and a maximal increase was observed with 50 nM CT, where pGL3-OT-luciferase activity was ~7-fold greater than that observed in vehicle-treated cells. The action of CT on pGL3-OT promoter was specific because CT did not alter luciferase activity of pGL3-OF, a mutant version of pGL3-OT where *LEF-1*-binding sites required for β-catenin-mediated action are mutated (36) (Fig. 7*C*). Next, we examined the effect of three different PKA inhibitors, (R_p)-cAMP (1 mM), m-PKI (100 nM), and H89 (3 μM) on CT-stimulated transcription. The results show that 50 nM CT stimulated luciferase activity by severalfold. However, CT failed to increase luciferase activity (pGL3-OT) in the presence of either of these inhibitors (Fig. 8, *A–C*). These data provide new evidence that CT stimulates β-catenin signaling in a PKA-dependent manner.

CT Inactivates GSK3β by Phosphorylation—Phosphorylation of GSK3 can disrupt the APC-AXIN2-GSK3β complex, stabilize cytosolic β-catenin, and enable its translocation into the nucleus (34). Because CT increased cytosolic and nuclear pools of β-catenin and stimulated β-catenin-mediated transcription, we examined a possibility that CT may accomplish this by GSK3 phosphorylation (37). PC-31-CTR cells were treated with 10 nM CT for various periods (0–4 h), and the lysates were collected and probed for the levels of phosphorylated GSK3β using phospho-GSK3β (Ser-21/9)-specific antibody (Cell Signaling, Boston). The antibody detects endogenous levels of GSK-3 only when phosphorylated at serine 21 of GSK3α or serine 9 of GSK3β. The levels of phosphorylated GSK3 remarkably increased in response to CT over a period of 4 h, with the initial increase as early as 1 h (Fig. 8*E*).

Because CT increased intracellular β-catenin levels, and stimulated β-catenin-responsive transcription in a PKA-dependent manner, we examined the role of PKA in CT-stimulated GSK3 phosphorylation. The results of Fig. 8*F* suggest that m-PKI almost abolished CTR-induced phosphorylation of GSK-3. It is conceivable that CTR-activated PKA may directly phosphorylate GSK3β (37).

However, it is also possible that CT may further increase GSK3β phosphorylation by activating the WNT signaling pathway (38). Therefore, we assessed CT-induced changes in the expression of WNTs and their receptors (FZD) by means of a WNT signaling pathway gene expression array. PC-31-CTR cells expressed the transcripts of ligands WNT1 and WNT3

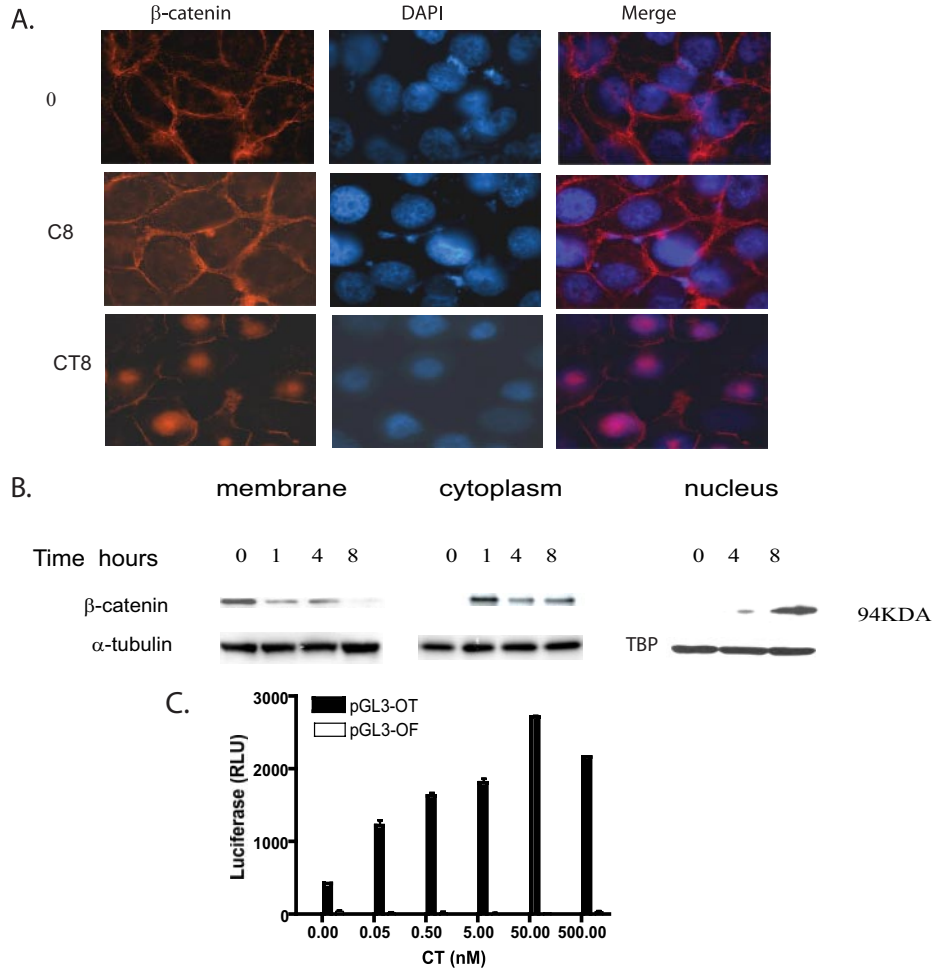

FIGURE 7. **Effect of CT-CTR axis on β-catenin translocation.** *A*, confluent monolayer of PC-31-CTR cells grown on transwell filters were allowed to polarize for 4 days. Serum-starved cells were treated with 50 nM CT for 8 h and fixed with methanol at −20 °C for 10 min. After immunostaining for β-catenin, pictures were captured at ×400. *Top* and *middle panels* show β-catenin localization in the membrane of PC-31-CTR treated with vehicle at 0 h (0) and 8 h (*C8*), respectively, whereas the *bottom panel* shows β-catenin translocated to the nucleus of PC-31-CTR cells when treated with CT for 8 h (*CT8*). *B*, effect of CT on β-catenin translocation. Confluent monolayers of PC-31 CTR cells were serum-starved and then treated with 50 nM of CT for periods of 0, 1, 4, and 8 h. Cells were first treated with cytosolic lysis buffer for 30 min to collect Triton X-100-soluble fraction. Then the remainder of the cells was treated with membrane lysis buffer to obtain Triton X-100-insoluble buffer. Nuclear fraction was extracted from four separate plates treated with CT for periods of 0, 4, and 8 h. Western blot analysis for β-catenin was carried out after loading 40 μg of cytosolic proteins and 20 μg of membrane and nuclear proteins. α-;tubulin, β-actin, and TATA-binding protein (*TBP*) were loading controls for membrane, cytoplasmic, and nuclear fractions, respectively. The experiment was repeated three separate times. *C*, effect of CT on TCF/LEF promoter activity. PC-31-CTR cells were seeded into 6-well plates and transfected with the pGL3-OT-luciferase/pRL-TK plasmids or pGL3-OF-luciferase/pRL-TK plasmids. The cells were then incubated in complete medium for 48 h, after which they were serum-starved for 16 h. The cells were then treated with various concentrations of CT (0–500 nM) for 8 h. The lysates were analyzed for luciferase activity. The results are expressed relative light units (*RLU*) after normalization with *Renilla* luciferase activity. The experiment was repeated three separate times. The results are expressed as means ± S.E.

and the receptors FZD1, FZD2, FZD8, and FZD10 (supplemental Table 1). CT remarkably increased the transcription of WNT1, with a smaller increase in WNT3 transcripts. CT also increased transcripts of other important components of WNT signaling pathway such as LRP6, disheveled 3 (DVL 3), and TCF/LEF proteins, suggesting the activation of canonical WNT signaling by the CT-CTR axis. Once again, the presence of m-PKI attenuated the actions of CT on WNT signaling, suggesting that PKA-mediated destabilization of cell-cell junctions may be a trigger for CT-stimulated WNT signaling. Moreover, the conditioned media harvested from the CT-stimulated PC-31-CTR cells enhanced TCF-mediated reporter activity, supporting the presence of increased concentrations of activators of β-catenin signaling such as WNTs in the conditioned media of CT-stimulated PC-31-CTR cells (Fig. 8*D*).

Taken together, these results suggest that CT stimulates a qualitatively durable GSK3 phosphorylation, which may result from direct phosphorylation of GSK3 by PKA as well as the activation of WNT signaling. Resulting accumulation of β-catenin in the nucleus leads to a more robust β-catenin-responsive transcriptional activity.

DISCUSSION

Earlier results from this laboratory have shown that the abundance of CT/CTR mRNA increases with tumor progression and correlates positively with the Gleason grade of primary prostate cancers (4). CTR, a G protein-coupled receptor, is a product of a single gene, but because of alternative splicing or post-translational processing of primary transcript, CTR has been reported to exist in at least six different isomeric forms (39). Human prostate expresses type 2 CTR, which lacks a 16-amino acid insert in the first intracellular loop, and is dually coupled to $G\alpha_s$ and $G\alpha_q$ proteins (30, 40, 41). However, $G\alpha_s$-activated, but not $G\alpha_q$-activated, signaling increases tumorigenicity of PC cell lines, and PKA plays a key role in CT-stimulated invasiveness of PC cell lines (18, 42). Acquisition of invasiveness by epithelial cancer cells is usually preceded by a phenomenon referred as EMT, which is characterized by the loss of some epithelial characteristics such as cell-cell adhesion, the ability to form multicellular structures, and the acquisition of migratory phenotype (12–14, 24, 43, 44). Therefore, we examined the role of the CT-CTR axis on the formation of acinar structures by PC cell lines in three-dimensional culture. Our results show that cell lines with inactive CT-CTR axis such as LNCaP, PC-3M-CT$^-$, and PC-3M-CTR$^-$ formed acinar structures. However, the same cell lines failed to form these structures when their CT-CTR axis was activated. Considering that acinar formation requires the cells to interact with each other and extracellular matrix to establish adhesion complexes, the results raised the

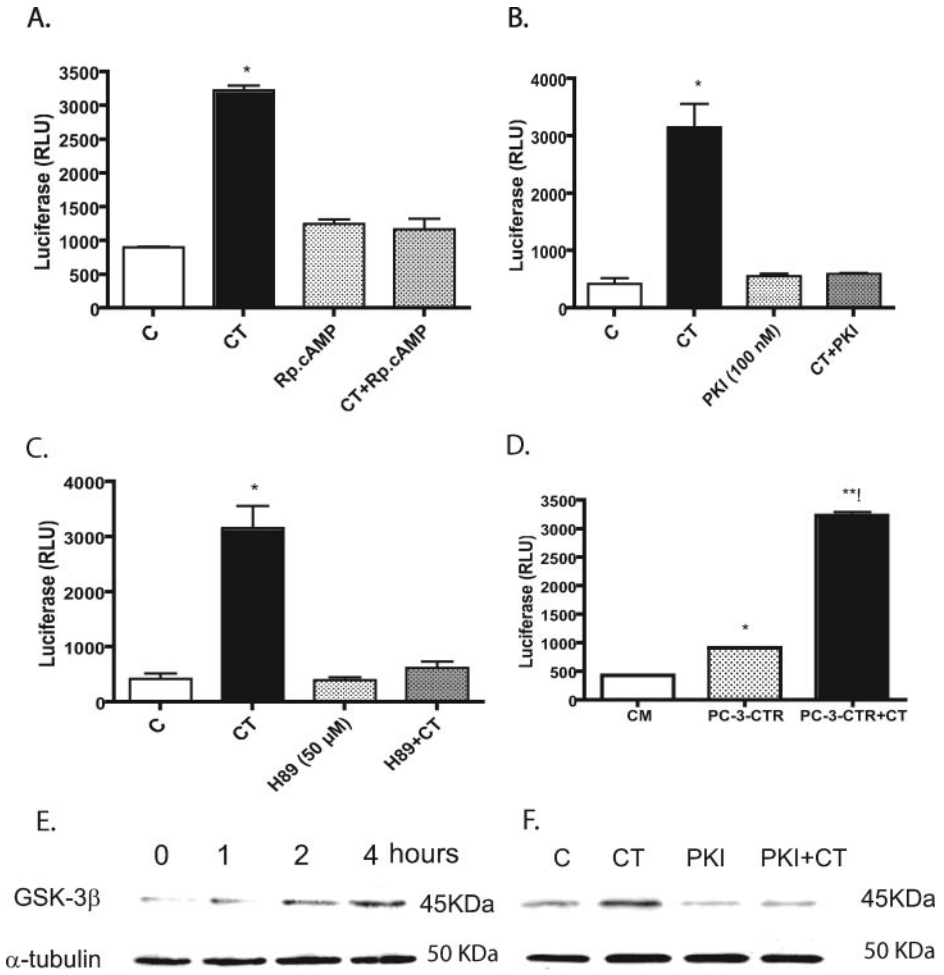

FIGURE 8. **Role for PKA in CT-stimulated transactivation of TCF/LEF promoter activity and GSK3β phosphorylation.** *A,* PC-31-CTR cells were seeded into 6-well plates and transfected with the pGL3-OT-luciferase and pRL-TK plasmids. The cells were then cultured in complete medium for 48 h, after which they were serum-starved for 16 h. The cells were then treated with either vehicle (*C*), 50 nM CT (*CT*), PKA inhibitor (R_p)-cAMP (*Rp-cAMP*) (1 mM), or 1 mM (R_p)-cAMP + 50 nM CT (*CT+Rp-cAMP*) for 8 h. The lysates were analyzed for luciferase activity. The results are expressed relative light units (*RLU*) after normalization with *Renilla* luciferase activity. The experiment was repeated three separate times. The results are expressed as mean ± S.E. *, $p < 0.05$ (one-way ANOVA and Newman-Keuls test). *B,* same as *A* except (R_p)-cAMP was replaced with another specific PKA inhibitor m-PKI (200 nM). *C,* same as *A,* except (R_p)-cAMP was replaced with PKA inhibitor H89 (3 μM). *D,* conditioned medium of CT-stimulated PC-3-CTR cells activates TCF-mediated transcription. PC-31-CTR cells were seeded into 6-well plates and transfected with the pGL3-OT-luciferase and pRL-TK plasmids. The cells were then cultured in complete medium for 48 h, after which they were serum-starved for 16 h. The cells were then incubated either with control medium (*CM*) or with the conditioned media harvested from 48-h cultured PC-31-CTR cells treated without/with 50 nM CT. The mean fold induction of five independent experiments is shown. *, $p < 0.05$ by Student's *t* test. *E,* PC-31-CTR cells were treated with 50 nM CT for 0, 1, 2, and 4 h. The cell lysates were collected. Western blot analysis for phopho-GSK-3β was carried out after loading 40 μg of total protein/lane. α-Tubulin was used as loading control. The experiment was repeated three separate times. *F,* PC-31-CTR cells were treated with vehicle (*C*), 50 nM CT (*CT*), 2 μM m-PKI (*PKI*), and with 2 μM m-PKI + 50 nM CT (*PKI+CT*) for 4 h. Western blot analysis for phospho-GSK-3β was carried out after loading 40 μg of protein collected from each treatment group. α-Tubulin was used as loading controls. The experiment was repeated three separate times.

possibility that the CT-CTR axis interferes with cell-cell adhesion (45, 46). Therefore, we examined cell-cell compaction patterns of PC sublines in two-dimensional cultures. All PC cell lines with inactive CT-CTR axis formed discrete colonies with epithelium-like cobblestone pattern where cells closely adhered to each other. However, activation of CT-CTR axis in these cell lines led to decreased cell-cell compaction and increased cell scattering.

Cell-cell adhesion is regulated by cell-cell contacts or junctions, which are functionally classified into three types, communicating junctions, adhesive junctions, and occluding junctions. The TJs are occluding junctions, which seal the cells together in an epithelial sheet, and are critical for the determination of epithelial cell polarity. Either disassembly or remodeling of TJs can cause a loss of cell polarity and an increase in motility (47, 48). AJs are adhesive contacts, which hold cells together in fixed position within the tissue. TJs along with AJs and desmosomes provide tissue integrity and promote cellular polarity, and AJ plays a pivotal role in regulating the entire activity of the junctional complex (47, 49). Our results suggest that the activation of CTR led to rapid remodeling of TJs as assessed by a large decrease in TER, an increase in paracellular permeability, and internalization of the key tight junction protein ZO-1 to the cytosol. The data from immunocytochemistry and immunoblotting studies corroborated these results and confirmed significant changes in TJ characteristics in response to CTR activation. CTR activation also led to the loss of AJs, loss of adhesive protein E-cadherin from membrane-associated fractions, and translocation of its partner protein β-catenin in the cytoplasmic compartment. Based on these results, it appears that CTR activation leads to rapid disassembly/remodeling of both TJ and AJ complexes and internalization of key junction proteins such as ZO-1 and β-catenin within minutes of CTR activation in a PKA-dependent manner. Considering that the loss of junctional complexes is associated with poor differentiation of other epithelial cancers (50, 51), and our recent results that activated CT-CTR axis increases metastasis of PC cells (4, 18), the present results raise the possibility that CTR-Gα_s-PKA-mediated junctional destabilization may play an important role in PC metastasis.

In addition to the destabilization of junctional complexes, activation of the CT-CTR axis also induced EMT in PC cell lines as demonstrated by the cadherin switch and the expression of the mesenchymal marker vimentin. E-cadherin, the major adhesion molecule in the AJs, is lost in epithelial cancers, including poorly differentiated prostate cancer and metastases (31, 52). Loss of E-cadherin is usually associated with the

appearance of N-cadherin in a phenomenon referred as "the cadherin switch" (53, 54). There is evidence to suggest that N-cadherin destabilizes cell-cell adhesion, which allows the cells to detach from the primary tumor and associate selectively with stroma and/or endothelium (55, 56). Other specific actions of N-cadherin include activation of Rho GTPases, mitogen-activated protein kinase (MAPK) pathways, and increased secretion of MMP-9 (57, 58). The present results that the activation of the CT-CTR axis in PC cell lines led to the loss of acinus-forming ability and cell-cell compaction and increased cell scattering and our earlier results that CT stimulated PC cell invasion and increased the secretion of MMP-2, MMP-9, and urokinase-type plasminogen activator from PC cell lines are consistent with the reported actions of N-cadherin (18, 20). Based on this evidence, one could hypothesize that CTR-mediated cadherin switch allows prostate cancer cells to scatter and acquire the invasive phenotype. Our results of Figs. 4–6 have also shown that inactivation of the CT-CTR autocrine loop reversed this process *in vitro* as well as in the xenografts of these cell lines *in vivo* by reverting the cells to epithelial phenotype, increasing E-cadherin, decreasing N-cadherin, and decreasing tumorigenicity (17). These results for the first time demonstrate that the activation of the CT-CTR axis induces EMT in PC cells, and that PKA-mediated junctional destabilization plays a key role in this process.

Activation of the CT-CTR axis in PC cell lines also caused internalization of β-catenin, the intracellular binding partner of E-cadherin (43). Internalized β-catenin is efficiently cleared by the APC-AXIN-GSK3β ubiquitination-proteasome degradation complex (59). Disruption of this complex can lead to accumulation of intracellular β-catenin, its translocation in the nucleus, and transcriptional activation of β-catenin-responsive genes (35). The present results that CT stimulated transactivation of pGL3-OT in a temporally consistent manner with the nuclear accumulation of β-catenin suggest that the CT-CTR axis may disrupt the APC-AXIN-GSK3β complex. Moreover, attenuation of CT-stimulated transactivation of pGL3-OT by protein kinase A inhibitors suggests that PKA plays a major role in this process.

Phosphorylation of GSK3β is an important mechanism to dissociate the APC-AXIN-GSK3β complex and stabilize intracellular β-catenin (37). Our results demonstrate that CT stimulated phosphorylation of GSK3 rapidly in a PKA-dependent manner. Although PKA can directly phosphorylate GSK3-β (60, 61), disheveled proteins, components of WNT signaling, are more potent agents of GSK3β phosphorylation (62). The present results that CT activates the canonical WNT signaling pathway by up-regulating WNT1 and -3, as well as several downstream proteins such as disheveled 3 and TCF/LEF transcriptional factors, suggest that CTR may phosphorylate GSK3β by more than one mechanism.

Our earlier studies have demonstrated that CTR is coupled to $G\alpha_s$ and activates PKA (30). Moreover, PKA plays a critical role in CT-stimulated invasion and metastasis of PC cell lines (17). Combining the present and previous findings, it appears that CT-CTR axis induces EMT of PC cell lines by activating the $G\alpha_s$-cAMP-PKA-mediated pathway as well as by destabilizing cell-cell contacts. Both these actions may be necessary for the activation of WNT/β-catenin-mediated transcription, a possibility supported by the evidence in other epithelial tumors (60, 61, 63).

Our results have important implications in understanding the pathology of PC progression. We have shown that metastatic and high grade PC tumors overexpress CT/CTR (4). In this study, we have shown that CTR activates WNT/β-catenin signaling. CTR-stimulated β-catenin signaling may support the progression of PC to the androgen-independent stage by transactivating androgen receptor-induced genes and genes responsible for EMT (64–66). Moreover, the β-catenin pathway is an important pathway for cell self-renewal (38, 64, 65) and may increase stemness of PC cells. Localization of CT/CTR expression in the basal epithelium where prostate stem cells are also localized supports this possibility (4, 66). Indeed, additional studies will be necessary to identify the precise molecular mechanisms where CTR and/or CTR-stimulated PKA-mediated mechanisms cross-talk with WNT/β-catenin signaling. However, these results provide novel biochemical explanation to our earlier observations and new therapeutic targets to arrest PC progression (17, 18).

In summary, we have presented several novel observations on the role of the CT-CTR axis in PC, and have identified a pathway that induces destabilization of junctional complexes, EMT, and activation of WNT/β-catenin signaling. These combined actions of CTR may explain its stimulatory actions on tumorigenicity and the invasiveness of PC cell lines.

Acknowledgment—We thank Dr. Bert Vogelstein for the gift of reporter plasmids pGL3-OT and pGL3-OF.

REFERENCES

1. Presti, J. C., Jr. (2000) *Radiol. Clin. North Am.* **38,** 49–58
2. Thompson, I. M., Pauler, D. K., Goodman, P. J., Tangen, C. M., Lucia, M. S., Parnes, H. L., Minasian, L. M., Ford, L. G., Lippman, S. M., Crawford, E. D., Crowley, J. J., and Coltman, C. A., Jr. (2004) *N. Engl. J. Med.* **350,** 2239–2246
3. Segawa, N., Mori, I., Utsunomiya, H., Nakamura, M., Nakamura, Y., Shan, L., Kakudo, K., and Katsuoka, Y. (2001) *Pathol. Int.* **51,** 452–459
4. Chien, J., Ren, Y., Qing Wang, Y., Bordelon, W., Thompson, E., Davis, R., Rayford, W., and Shah, G. (2001) *Mol. Cell. Endocrinol.* **181,** 69–79
5. Furuya, Y., Akakura, K., Akimoto, S., Inomiya, H., and Ito, H. (1999) *Int. J. Urol.* **6,** 240–244
6. Cooper, C. R., and Pienta, K. J. (2000) *Prostate Cancer Prostatic Dis.* **3,** 6–12
7. Torer, N., Kayaselcuk, F., Nursal, T. Z., Yildirim, S., Tarim, A., Noyan, T., and Karakayali, H. (2007) *J. Surg. Oncol.* **96,** 419–423
8. Acevedo, V. D., Gangula, R. D., Freeman, K. W., Li, R., Zhang, Y., Wang, F., Ayala, G. E., Peterson, L. E., Ittmann, M., and Spencer, D. M. (2007) *Cancer Cell* **12,** 559–571
9. Hugo, H., Ackland, M. L., Blick, T., Lawrence, M. G., Clements, J. A., Williams, E. D., and Thompson, E. W. (2007) *J. Cell. Physiol.* **213,** 374–383
10. Xu, J., Wang, R., Xie, Z. H., Odero-Marah, V., Pathak, S., Multani, A., Chung, L. W., and Zhau, H. E. (2006) *Prostate* **66,** 1664–1673
11. Rosano, L., Spinella, F., Di Castro, V., Nicotra, M. R., Dedhar, S., de Herreros, A. G., Natali, P. G., and Bagnato, A. (2005) *Cancer Res.* **65,** 11649–11657
12. Vandewalle, C., Comijn, J., De Craene, B., Vermassen, P., Bruyneel, E., Andersen, H., Tulchinsky, E., Van Roy, F., and Berx, G. (2005) *Nucleic Acids Res.* **33,** 6566–6578
13. Maeda, M., Johnson, K. R., and Wheelock, M. J. (2005) *J. Cell Sci.* **118,** 873–887

14. Eger, A., Stockinger, A., Park, J., Langkopf, E., Mikula, M., Gotzmann, J., Mikulits, W., Beug, H., and Foisner, R. (2004) *Oncogene* **23,** 2672–2680
15. Yang, A. D., Camp, E. R., Fan, F., Shen, L., Gray, M. J., Liu, W., Somcio, R., Bauer, T. W., Wu, Y., Hicklin, D. J., and Ellis, L. M. (2006) *Cancer Res.* **66,** 46–51
16. Grande, M., Franzen, A., Karlsson, J. O., Ericson, L. E., Heldin, N. E., and Nilsson, M. (2002) *J. Cell Sci.* **115,** 4227–4236
17. Thomas, S., Chigurupati, S., Anbalagan, M., and Shah, G. (2006) *Mol. Endocrinol.* **20,** 1894–1911
18. Sabbisetti, V. S., Chirugupati, S., Thomas, S., Vaidya, K. S., Reardon, D., Chiriva-Internati, M., Iczkowski, K. A., and Shah, G. V. (2005) *Int. J. Cancer* **117,** 551–560
19. Shah, G. V., Shibu, T., Anbalagan, M., Yong Liu, P. L., Hermonat, J. W., and Jaideep, C. (2008) *Endocr.-Relat. Cancer* **15,** 1–15
20. Sabbisetti, V. S., Chigurupati, S., Thomas, S., and Shah, G. V. (2005) *Int. J. Cancer* **118,** 2694–2702
21. Kaighn, M. E., Narayan, K. S., Ohnuki, Y., Lechner, J. F., and Jones, L. W. (1979) *Investig. Urol.* **17,** 16–23
22. Lim, D. J., Liu, X. L., Sutkowski, D. M., Braun, E. J., Lee, C., and Kozlowski, J. M. (1993) *Prostate* **22,** 109–118
23. Chigurupati, S., Kulkarni, T., Thomas, S., and Shah, G. (2005) *Cancer Res.* **65,** 8519–8529
24. Lang, S. H., Stark, M., Collins, A., Paul, A. B., Stower, M. J., and Maitland, N. J. (2001) *Cell Growth & Differ.* **12,** 631–640
25. Thomas, S., Muralidharan, A., and Shah, G. V. (2007) *Int. J. Oncol.* **31,** 1425–1437
26. Thomas, S., and Shah, G. (2005) *Cancer Biol. Ther.* **4,** 1226–1233
27. Bello-DeOcampo, D., Kleinman, H. K., Deocampo, N. D., and Webber, M. M. (2001) *Prostate* **46,** 142–153
28. Tsukita, S., Furuse, M., and Itoh, M. (1996) *Cell Struct. Funct.* **21,** 381–385
29. Anderson, J. M., and Van Itallie, C. M. (1995) *Am. J. Physiol.* **269,** G467–G475
30. Chien, J., and Shah, G. V. (2001) *Int. J. Cancer* **91,** 46–54
31. Hirohashi, S., and Kanai, Y. (2003) *Cancer Sci.* **94,** 575–581
32. Sakakibara, A., Furuse, M., Saitou, M., Ando-Akatsuka, Y., and Tsukita, S. (1997) *J. Cell Biol.* **137,** 1393–1401
33. Sommers, C. L., Heckford, S. E., Skerker, J. M., Worland, P., Torri, J. A., Thompson, E. W., Byers, S. W., and Gelmann, E. P. (1992) *Cancer Res.* **52,** 5190–5197
34. Ha, N. C., Tonozuka, T., Stamos, J. L., Choi, H. J., and Weis, W. I. (2004) *Mol. Cell* **15,** 511–521
35. Mann, B., Gelos, M., Siedow, A., Hanski, M. L., Gratchev, A., Ilyas, M., Bodmer, W. F., Moyer, M. P., Riecken, E. O., Buhr, H. J., and Hanski, C. (1999) *Proc. Natl. Acad. Sci. U. S. A.* **96,** 1603–1608
36. Shih, I. M., Yu, J., He, T. C., Vogelstein, B., and Kinzler, K. W. (2000) *Cancer Res.* **60,** 1671–1676
37. Fang, X., Yu, S. X., Lu, Y., Bast, R. C., Jr., Woodgett, J. R., and Mills, G. B. (2000) *Proc. Natl. Acad. Sci. U. S. A.* **97,** 11960–11965
38. Katoh, M., and Katoh, M. (2007) *Clin. Cancer Res.* **13,** 4042–4045
39. Moore, E. E., Kuestner, R. E., Stroop, S. D., Grant, F. J., Matthewes, S. L., Brady, C. L., Sexton, P. M., and Findlay, D. M. (1995) *Mol. Endocrinol.* **9,** 959–968
40. Shah, G. V., Rayford, W., Noble, M. J., Austenfeld, M., Weigel, J., Vamos, S., and Mebust, W. K. (1994) *Endocrinology* **134,** 596–602
41. Wu, G., Burzon, D. T., di Sant'Agnese, P. A., Schoen, S., Deftos, L. J., Gershagen, S., and Cockett, A. T. (1996) *Urology* **47,** 376–381
42. Chien, J., Wong, E., Nikes, E., Noble, M. J., Pantazis, C. G., and Shah, G. V. (1999) *Oncogene* **18,** 3376–3382
43. Jankowski, J. A., Bruton, R., Shepherd, N., and Sanders, D. S. (1997) *Mol. Pathol.* **50,** 289–290
44. Ikenouchi, J., Matsuda, M., Furuse, M., and Tsukita, S. (2003) *J. Cell Sci.* **116,** 1959–1967
45. Hall, H. G., Farson, D. A., and Bissell, M. J. (1982) *Proc. Natl. Acad. Sci. U. S. A.* **79,** 4672–4676
46. Reginato, M. J., Mills, K. R., Becker, E. B., Lynch, D. K., Bonni, A., Muthuswamy, S. K., and Brugge, J. S. (2005) *Mol. Cell. Biol.* **25,** 4591–4601
47. Thiery, J. P., Boyer, B., Tucker, G., Gavrilovic, J., and Valles, A. M. (1988) *CIBA Found. Symp.* **141,** 48–74
48. Hurd, T. W., Gao, L., Roh, M. H., Macara, I. G., and Margolis, B. (2003) *Nat. Cell Biol.* **5,** 137–142
49. Keiper, T., Santoso, S., Nawroth, P. P., Orlova, V., and Chavakis, T. (2005) *Histol. Histopathol.* **20,** 197–203
50. Martin, T. A., Watkins, G., Mansel, R. E., and Jiang, W. G. (2004) *Eur. J. Cancer* **40,** 2717–2725
51. Tyagi, N., Sharma, S., Tyagi, S. P., Maheshwari, V., Nath, P., Ashraf, S. M., and Srivastava, A. N. (1993) *J. Postgrad. Med.* **39,** 197–201
52. Otto, T., Rembrink, K., Goepel, M., Meyer Schwickerath, M., and Rubben, H. (1993) *Urol. Res.* **21,** 359–362
53. Gravdal, K., Halvorsen, O. J., Haukaas, S. A., and Akslen, L. A. (2007) *Clin. Cancer Res.* **13,** 7003–7011
54. Jaggi, M., Johansson, S. L., Baker, J. J., Smith, L. M., Galich, A., and Balaji, K. C. (2005) *Urol. Oncol.* **23,** 402–406
55. Tsukamoto, T., and Nigam, S. K. (1999) *J. Biol. Chem.* **274,** 24579–24584
56. Nakajima, S., Doi, R., Toyoda, E., Tsuji, S., Wada, M., Koizumi, M., Tulachan, S. S., Ito, D., Kami, K., Mori, T., Kawaguchi, Y., Fujimoto, K., Hosotani, R., and Imamura, M. (2004) *Clin Cancer Res.* **10,** 4125–4133
57. Suyama, K., Shapiro, I., Guttman, M., and Hazan, R. B. (2002) *Cancer Cell* **2,** 301–314
58. Hazan, R. B., Qiao, R., Keren, R., Badano, I., and Suyama, K. (2004) *Ann. N. Y. Acad. Sci.* **1014,** 155–163
59. Fuchs, S. Y. (2002) *Cancer Biol. Ther.* **1,** 337–341
60. Suzuki, A., Ozono, K., Kubota, T., Kondou, H., Tachikawa, K., and Michigami, T. (2008) *J. Cell. Biochem.* **104,** 304–317
61. Hino, S., Tanji, C., Nakayama, K. I., and Kikuchi, A. (2005) *Mol. Cell. Biol.* **25,** 9063–9072
62. Polakis, P. (2000) *Genes Dev.* **14,** 1837–1851
63. Gaujoux, S., Tissier, F., Groussin, L., Libe, R., Ragazzon, B., Launay, P., Audebourg, A., Dousset, B., Bertagna, X., and Bertherat, J. (2008) *J. Clin. Endocrinol. Metab.* **93,** 4135–4140
64. Campbell, C., Risueno, R. M., Salati, S., Guezguez, B., and Bhatia, M. (2008) *Curr. Opin. Hematol.* **15,** 319–325
65. He, B., and Jablons, D. M. (2006) *Ernst. Schering Found. Symp. Proc.* **5,** 27–58
66. Lam, J. S., and Reiter, R. E. (2006) *Urol. Oncol.* **24,** 131–140